PERGAMON

Journal of Atmospheric and Solar-Terrestrial Physics 62 (2000) 189–206

Journal of ATMOSPHERIC AND SOLAR-TERRESTRIAL PHYSICS

Trimpi perturbations from large ionisation enhancement patches

D. Nunn[a,*], H.J. Strangeways[b]

[a]*Department of Electronics and Computer Science, University of Southampton, Highfield, Southampton SO17 1BJ, UK*
[b]*School of Electronic and Electrical Engineering, University of Leeds, Leeds LS2 9JT, UK*

Received 10 September 1999; received in revised form 25 November 1999; accepted 30 November 1999

Abstract

A number of increasingly sophisticated and realistic models have been developed in order to investigate the interaction between sub-ionospherically propagating VLF waves and regions of ionisation enhancement (LIE[1]) in the D-region caused by lightning-induced electron precipitation enhancements (LEP). This LEP-produced LIE can result in phase and amplitude perturbations on received VLF radio signals that are referred to as Trimpis or more precisely, classic Trimpis, to distinguish them from "early/fast Trimpis" or "VLF sprites" which are not caused by LEP and are not considered here. It is important, for comparison with experimentally observed Trimpi effects, that the spatial extent of the D-region electron density (N_e) perturbation is modeled accurately. Here, it is argued that most previous modeling has used patch (LIE) sizes that are typically up to 100 km in both latitudinal and longitudinal extent, which are generally smaller than those that actually occur for real lightning induced electron precipitation events. It would also appear that maximum ΔN_e values assumed have often been too large, and the patches (LIEs) have been incorrectly modelled as circular rather than elliptical in horizontal extent. Consequently, in the present work, Trimpi perturbations are determined for LIEs with smaller maximum ΔN_e, larger spatial extent and elliptical shape. Calculations of VLF Trimpis have been made as a function of the horizontal coordinates of the LIE centre, over the whole rectangular corridor linking transmitter and receiver. The Trimpi modelling program is fully 3D, and takes account of modal mixing at the LIE. The underlying theory assumes weak Born scattering, but the code calculates a non-Born skin depth attenuation function for the LIE in question. The LIE is modelled as an electron density enhancement with a Gaussian profile in all coordinates. Results for a large elliptical LIE $\sim 200 \times 600$ km show that significant Trimpis, ~ -0.4 dB in amplitude and $\sim +4^\circ$ in phase are predicted, using modest maximum ΔN_e values ~ 1.5 el/cc. Such an electron density enhancement is well within the range that would be expected to result from experimentally observed fluxes of electron precipitation following wave particle interactions with whistler-mode waves.

1. Introduction

Helliwell et al. (1973) were the first to report night-time changes associated with whistlers in the amplitude of long distance sub-ionospheric VLF transmissions from NSS, Annapolis, Maryland (on 22.3 kHz) and NAA, Cutler, Maine (on 18.6 kHz) to Eights and Byrd

* Corresponding author. Tel: +44-23-8059-2075.
E-mail address: dn@ecs.soton.ac.uk (D. Nunn).

[1] The "L" in "LIE" stands for "LEP-produced"

1364-6826/00/$ - see front matter
PII: S1364-6826(00)00004-3

stations in Antarctica. Each enhancement began with a relatively fast (1–3 s) rise in amplitude of up to 6 dB followed by a slower recovery lasting 10–40 s. Both increases and decreases in signal amplitude were observed depending on signal frequency and orientation of the receiving antenna. Coincident with every amplitude perturbation was a mid-latitude whistler originating in the northern hemisphere. Thus the phenomenon was explained by the whistler precipitating energetic (30–300 keV) electrons into the D-region, the resulting ionisation then altering the properties of the Earth-ionosphere waveguide. The precipitation mechanism was thought to be the result of pitch angle scattering following transverse cyclotron resonance of the ducted whistler waves with counterstreaming energetic electrons within the interaction region, which covers a few 1000 km either side of the equatorial plane. The resonant interaction decreases the kinetic energy perpendicular to the geomagnetic field for some electrons, causing them to enter the loss cone.

Phase advances and decreases on sub-ionospheric VLF transmissions, similarly associated with whistlers, were later reported by Lohrey and Kaiser (1979). These were explained by a two mode Earth-ionosphere waveguide propagation model which was also shown to account for the amplitude changes seen by Helliwell et al. (1973). The same basic mechanism of whistler-induced particle precipitation locally increasing D-region ionisation was adopted. It was shown that larger phase perturbations would result for a receiver location where the two most significant waveguide modes nearly cancelled. Further experimental results confirmed that Trimpi perturbations were generally observed as a night-time phenomenon (Leyser et al., 1984), since in the daytime the lower VLF reflection height results in a much weaker scattered signal and renders Trimpis below the noise floor except for very strong events. Trimpi observations were extended to lower latitudes (Carpenter and LaBelle, 1982), more easterly longitudes (Friedel and Hughes, 1990) and to higher (LF, MF) frequencies (Carpenter et al., 1984).

Modelling of the effect of LIEs on sub-ionospheric VLF propagation is important for a detailed understanding of experimental data on Trimpi amplitude and phase perturbations and their variation with transmitter frequency, transmitter-receiver path length and LIE location with respect to the transmitter-receiver great circle (GC) path. More recent modelling includes LIEs of finite lateral extent, located on and off the transmitter-receiver path and mode conversion both along the path and at the LIE location. Numerical simulations are important in order to be able to quantify the amplitude and phase perturbations expected for a given transmitter frequency and transmitter-receiver path when one or more LIEs lie along it or close to it. Early modelling of this scenario (Tolstoy, 1983; Inan et al., 1985; Tolstoy et al., 1982; Inan and Carpenter, 1987) was generally restricted to a 2D Earth-ionosphere waveguide model, infinite and homogeneous in the direction transverse to the propagation path. Thus, the LIE was assumed to lie directly on the path and extend to infinity both sides of it. Tolstoy et al. (1982) found from their model that small increases in amplitude would occur for LIEs near the transmitter or receiver. Large perturbations in amplitude (>3 dB) appeared to require LIEs near both the transmitter and the receiver. Further work by Tolstoy and Rosenberg (1986) employed a more realistic propagation model including multiple modes, variable ground conductivity and mode conversion, and considered LIE regions of variable length (typically 50–150 km) and distances from transmitter to receiver of up to 600 km. These calculations showed that some signal paths were more sensitive to perturbations than others and that the size of a LIE region was less important than its distance from the receiver. The model employed in both papers, being 2D, was restricted to perturbations directly on the transmitter-receiver path. However, it is important to consider modal interference when explaining classical Trimpis. With particular reference to the path NWC to Dunedin, Dowden and Adams (1989b) argued for this as follows. Interference between the first two modes of Earth-ionosphere waveguide propagation in the top half of the VLF band (>18 kHz) increases with distance from the transmitter out to very large distances and can modify amplitude and phase perturbations produced by LIEs. For frequencies greater than 18 kHz, the first order mode has an "Earth detached" character in that successive reflections occur from the ionosphere without intermediate ground reflections. For a transmitter on the ground, excitation of the first mode is 20 dB less than the second at around 22 kHz. Thus, since the second mode is attenuated more than the first, amplitudes will eventually become comparable producing strong modal interference. Then, since the two modes correspond to slightly different phase velocities, an interference pattern or standing wave is formed which is shifted slightly along the path by the LIE-induced change in differential phase velocity. The modal effect at the receiver therefore depends on the local gradient of amplitude along the transmitter-receiver path. This conclusion was in agreement with Lohrey and Kaiser (1979) who showed that all the Trimpi related modal effects (except for the unique case of almost complete cancellation of the two mode phasors) are due to displacement of this spatial interference pattern along the path through the receiver. Since this differential phase depends on frequency, measurement of the resultant amplitude at two close frequencies permits an estimation of the modal effects. This was accomplished using the two sidebands 22,250 Hz and 22,350 Hz of

the NWC MSK transmitter during a night of frequent Trimpis. The geometry could be considered to be 2D, with Trimpis produced by large area LIEs spanning the transmitter-receiver path. It was found that the Trimpi amplitude and phase were related to the local gradient of signal strength amplitude as expected. Further, it was deduced that modal modifications of Echo Trimpis would be insignificant. Cotton and Smith (1991), using Trimpi data for the West-East Siple-Halley path, provided evidence for elongated disturbances lying close to and parallel with the path (similar to the observations of Dowden and Adams (1989a)).

The modelling of Trimpi perturbations was extended to 3D by Poulsen et al. (1990). Their model enabled the effect of LIE regions of finite size both on and to the side of the transmitter-receiver path to be investigated. This also enabled them to link the ratio of amplitude and phase perturbations at the receiver to the distance of the LIE from the transmitter-receiver path. Their model was, however, restricted to a single mode but was extended to include multi-moded propagation by Poulsen et al. (1993a). The long wave propagation model (LWPM) took into account realistic ground and ionosphere conductivity variation in the horizontal plane that results in continuous mode conversion along all propagation paths. Mode conversion due to scattering at the LIE was not, however, included. The model was applied to experimental observations and generally found to be in good agreement. Poulsen et al. (1993b) also used the 3D model to investigate the effect of the conductivity and permittivity of the Earth in the vicinity of the D-region perturbation. They found that the scattering was independent of these parameters except for very low conductivities such as those over deep ice caps. Assuming that the strength of the ionospheric modification (the LIE) decreases laterally from the centre following a Gaussian form, they also determined the beam width of the scattered signal and found that most of the wave energy scatters within a fairly narrow angular region (15 dB beamwidth of $\pm 7^{\circ}$ for a disturbance radius of 100 km) centred on the forward scatter direction. Thus they concluded that moderate to large-scale disturbances (radius 50–200 km) must be situated within < 250 km of a GC path of moderate length (3000–16,000 km) in order to scatter a measurable signal to the receiver. A similar conclusion was drawn in a much earlier paper by Crombie (1964).

These authors noted that their treatment assumed that each modal field satisfies the WKB approximation within the perturbed region and that no significant modal coupling takes place in the LIE. Such mode conversion was investigated by Wait (1995) for VLF scattering from a column of ionisation in the Earth-ionosphere waveguide, making use of his earlier work (Wait, 1980). He found significant mode conversion where the ionisation was limited in height or a function of height. Nunn (1997) considered that a fundamental assumption underlying the treatments of Poulsen et al. (1990, 1993a, 1993b) was invalid; since the perturbation scale was of the order of the VLF wavelength, intermodal coupling at the LIE could not be neglected. It was argued that, since the dominant TM modes have equivalent complex indices of refraction within a few percent of one another, it would need LIE sizes of $\gg 1000$ km to eliminate inter-modal coupling. Nunn's (1997) treatment is based on a multimodal treatment of an assembly of point scatterers and is subject to the Born weak scattering approximation.

Baba and Hayakawa (1995, 1996) also considered cross-modal scattering at the LIE in their treatment of the effect of localised perturbations in the lower ionosphere on sub-ionospheric propagation. They employed a finite element method (FEM) but due to the complexity of this method analysed only the 2D case where a localised perturbation lay on the GC path between the transmitter and the receiver. The incident field was just considered to be that due to the first order mode. The redistribution of energy from this first order mode into higher modes due to the perturbation was determined. A particular advantage of their method is that it does not rely on the Born approximation, is valid for all patch geometries and is accurate at altitudes up to 120 km. Calculations up to 600 km downstream from the LIE using the FEM method revealed oscillations in the perturbations of VLF amplitude and phase. These were considered to arise from mode conversion and subsequent multiple mode propagation. Comparison between calculations using their FEM treatment and a 3D code that invokes the Born approximation was made by Nunn et al. (1998). The results from the two computations showed excellent agreement. For an LIE with a horizontal extent of 100 km they showed that departure from the linear Born approximation behaviour would occur at a maximum electron density enhancement of about 6 el/cc. In the present work, the maximum enhancement employed will be 1.5 el/cc, well within the Born limit even for the larger LIE patches employed.

2. LIE imaging

Observations, of VLF perturbations on adjacent paths can be used to estimate LIE sizes and positions, and can thus be regarded as imaging LIEs. Networks of paths have also been established by co-operation between two or more research groups, e.g., OPALnet incorporated a network of receivers run by both

British Antarctic Survey and the Physics Department at the University of Otago. Larger networks enable simultaneous observations of Trimpis over more paths and thus help to determine more precisely the area around an LIE over which VLF paths are significantly perturbed. Inan et al. (1990) conducted such an investigation using simultaneous observations in California, Saskatchewan and Quebec of VLF signals from multiple transmitters, allowing the monitoring of event activity over a coarse grid covering the USA. Occurrence statistics of simultaneous events on crossing paths were consistent with spatial extents of the disturbed ionosphere regions (LIEs) of less than a few hundred km. The relatively low occurrence of simultaneous events on adjacent paths suggested that scattering from disturbances off the great circle path (by >100 km) was not significant. Dowden and Adams (1988) explained phase and amplitude perturbations of the NWC transmitter received at Dunedin in terms of very compact or multiple LIEs and termed these Echo Trimpis. Extended or multiple LIEs would be more likely to exist for this path since part of it, in the Tasman Sea area, was nearly tangential to a line of constant L-shell and ducts are believed to have significantly greater extent in the longitudinal than in the latitudinal direction. Dowden and Adams (1989a) reported a more extensive set of observations. Diffraction regions were determined to be up to 200 km from the great circle path and, although less than 50 km wide in latitude, were considered to be considerably elongated along L-shells.

Dowden et al. (1993) distinguished between GCP (great circle path) Trimpis produced by large and/or smoothly varying LIEs which straddle the transmitter-receiver path and echo Trimpis produced by scattering from small or structured LIEs situated off the GC path. It now seems likely that their echo Trimpis were due to VLF sprites and only their GCP Trimpis were the LEP-produced classic Trimpis of interest here. They argued that, for GCP Trimpis, causative LIEs can be located and mapped by geometric optics using a network of receivers of sufficient density (spacing $\sim$ 100 km) and a few transmitters. Dowden et al. (1993) presented observations of Trimpi perturbations over the length of a 600 km array consisting of five Trimpi receivers and interpreted the results in terms of different models of the LIEs. Seventy Trimpi events, observed on all five array elements during a single night, were used to determine LIE location and size, and to test the applicability of the different LIE models. Most LIEs had North–South dimensions of 100–250 km but much larger East–West dimensions, and it was suggested that this accounted for the very strong Trimpis observed. Dowden et al. (1993) concluded that about half of the LIEs could have had a smooth (e.g. Gaussian) lateral spread. The remainder required varying degrees of fine structure from flat or Butterworth shapes to multiple LIEs (that might result from multiduct whistlers) to explain the observed diffraction patterns exhibiting maxima and minima, as well as the wide scattering angle implied by the observed simultaneous Trimpis.

Smith et al. (1993) described the characteristics and statistics of Trimpis observed in the Antarctic Peninsula region. The amplitude and phase of four Omega transmitters were recorded in each transmission quadrant and a 12 month long data set scanned for Trimpis. A scatter plot of Trimpi amplitude versus phase for the all-sea Hawaii to Faraday path was interpreted to infer that the LEP regions responsible for the events occurred predominantly in the L-range 2–3, with the horizontal size of the perturbed region of the ionosphere being typically 50 km latitudinally and 200 km longitudinally.

2.1. Duct dimensions

This greater East–West than North–South dimension is thus in agreement with the observations made by Dowden et al. (1993), who inferred the duct extent in the equatorial plane to be four to eight times greater in longitude than latitude. However, duct dimensions determined in situ by satellites, from the spatial extent of observed whistlers with constant dispersion, are generally significantly smaller when projected to low altitude than those that would be inferred from the extent of LEP bursts or estimated LIE patch sizes. For example, OGO 3 observations of some whistler ducts in the range $L = 4.1$–4.7 showed thicknesses from 0.035 to 0.07 Earth radii (Angerami, 1970) in the magnetic meridional direction, corresponding to 223–446 km. Low altitude satellite observations at about 2000 km altitude (Ondoh, 1976) showed an occurrence maximum in the range 10–20 km. The low and high altitude wave duct widths are not inconsistent taking into account the effect of the spreading out of the field lines. At $L = 4$, for example, a duct has a latitudinal width in km (measured across the duct) 16 times greater in the equatorial plane than at 2000 km altitude so that the width range measured by OGO 3 would map to 14–28 km. The shape of the duct cross-section will also vary along the duct length. A circular cross-section at the equator would map to an elliptical cross-section at low altitude (with the major axis in the longitude direction as this dimension varies linearly with altitude whereas the latitudinal extent varies approximately as the square of altitude). Clearly the low altitude duct widths are much smaller than those $\sim$100 km or more observed for LEP bursts at low altitude (Voss et al., 1998) or the horizontal extent inferred for LIEs of up to 300 km. It can be concluded that both

low altitude satellite observations of precipitating electron bursts and estimates of the extent of LIEs by Trimpi perturbations on nearby propagation paths imply a horizontal extent in the latitudinal direction of about 100–300 km, whereas observations of the spatial extent of whistlers of constant dispersion observed on the ground by triangulation or by low altitude satellite (or high altitude satellite and projected down to low altitude) imply duct widths of about 10–30 km in the latitudinal direction, an order of magnitude smaller than the LIE or LEP burst extent.

2.2. Wave and precipitation duct widths

Strangeways (1999) investigated this discrepancy by ray-tracing in a variety of 3D duct models. Calculations made for ducts, with maximum enhancement and width in ΔL-value constant along their length, imply that precipitation regions and LIEs would typically have significantly smaller dimensions in L-value than low altitude whistler duct widths measured by the spatial extent of the whistler-mode waves. However, this appears to be contrary to experimental observations. Therefore, to account for this discrepancy in duct width, ray paths were also determined for ducts which vary in enhancement and/or width in ΔL-value along their length. Although a better fit with experimental observations is obtained for such ducts, there were shown to be problems in explaining LIE patch sizes significantly *wider* in L-value than duct sizes implied from the spatial extent of whistlers with constant dispersion. The spatial extent of the LEP is strictly a measure of the lateral extent (in ΔL-value or longitude) of the equatorial interaction region. Thus the most straightforward way of explaining this discrepancy, as first suggested by Strangeways (1997), is to assume that the interaction region extends beyond the lateral limits of the duct. This could come about by the currents produced by the trapped particles in gyroresonance re-radiating whistler-mode wave energy from the duct to the outer regions beyond the duct. This 'non-linear unducting loss' occurs in the equatorial interaction region. Nunn (1984) found from numerical modeling of the wave–particle interaction that the generation region solution requires a high degree of power loss (80–95% of input power); this provides a saturation mechanism and serves to stabilise the generation region structure. He found that, as a consequence of the non-linear wave–particle interaction, the resonant particle current is a function of the transverse co-ordinates x and y which causes phase variations in the plane perpendicular to the geomagnetic field direction. This non-linear resonant current in the interaction region then radiates power into modes with larger wave normal angles than those of the original ducted waves. The energy associated with these modes will leak from the duct and will tend to fill the outer and surrounding region of the duct. If, then, particle precipitation occurs over this larger region, the duct as measured by precipitating electrons would be larger than the region of enhanced electron density. The above explanation is strengthened by the observations by Angerami (1970) of the presence of leaked whistler-mode signals beyond the confines of the ducts in which they appear to have previously propagated. This wave-energy was considered by Angerami (1970) to be the result of the half gyrofrequency cut-off for ducts of enhanced ionisation. Wave energy above half the local electron gyrofrequency may contribute to precipitation outside the bounds of the enhancement duct as frequencies in this range could either be just leaking away from the duct or guided in regions of reduced electron density (troughs) outside the enhancement duct or between closely spaced enhancement ducts. For frequencies below half the equatorial gyrofrequency, which will be more important, non-linear unducting loss will be the dominant mechanism for spreading wave energy in the equatorial region beyond the confines of the duct as defined by its enhanced electron density.

2.3. The LIE scattering model

The transmission path under consideration is that from NWC in NW Australia to Dunedin in New Zealand, a path length of 5.74 Mm. The transmitter NWC is modelled as a vertical electric dipole at zero altitude, transmitting at 19.8 kHz. The receiver at Dunedin is assumed to be a vertical electric dipole, though in experimental practice the horizontal magnetic fields are measured. The computer code for the numerical modeling of Trimpis is fully three dimensional with an anisotropic ionosphere and curved Earth, and is based upon a linear weak scattering (Born) formalism. The code is very general and has been used successfully to model VLF scattering from a time decaying red sprite plasma column (Nunn and Rodger, 1999) and also from assemblies of spritelet plasma columns (Rodger and Nunn, 1999). Apart from the LIE itself the background ionosphere is assumed to be homogeneous. Both the ionosphere and the ground are assumed to have properties that are an average of those along the path NWC-Dunedin. The ionospheric electron density and collision frequency profiles are given by a standard nightime ionospheric model. The collision frequency profile is given by

$$\nu(z) = 1/\tau(z) = 1.86 \times 10^{11}\, \mathrm{e}^{-0.15z}\ \mathrm{s}^{-1} \quad (1)$$

and the unperturbed electron density profile given by

$$N_e(z) = (7.857 \times 10^{-5})\, e^{\beta(z-h)} \nu(z)/\text{cc} \quad (2)$$

where we take $\beta = 0.5$ km^{-1} and $h = 84$ km. The ground is assumed homogeneous with an average conductivity of 0.01 $\mho$/m and average dielectric dielectric constant of 15. The ambient magnetic field is assumed to have a strength of 5.7×10^{-5} T and a co-dip angle of 24°.

The LIE is defined by the quantity $\delta N_e(x, y, z)$ or the perturbation of electron density. The perturbation of collision frequency $\delta\nu(x, y, z)$ due to heating is assumed zero due to the rapid cooling of the plasma within a time scale ~ms. The LIE may then be defined as a spatial perturbation of susceptibility tensor $X'(x, y, z)$. LIE electron density profile $\delta N_e(x, y, z)$ is assumed to have a Gaussian dependence on horizontal coordinates x and y, and in accordance with the above discussion to be elliptically shaped with the long axis along magnetic E/W. The vertical dependence of the electron density perturbation is also assumed to be Gaussian, centred at a height z_0 with a variance σ. We thus have

$$\delta N_e = \delta N_e^0 \cdot \exp\Big[(z - z_0)^2/\sigma^2 + \left(x' - x_0'\right)^2/S_x^2 + \left(y' - y_0'\right)^2/S_y^2\Big] \quad (3)$$

where x' is the local E/W coordinate and y' is the N/S coordinate. In the present simulation, we take $z_0 = 75$ km and $\sigma = 10$ km. The E/W variance S_x^2 is taken to be (300 km)^2 and the N/S variance S_y^2 = (100 km)^2, giving an ellipticity of 3. In the vertical direction, the LIE is limited to the height range 50–86 km. The top height of 86 km is above the reflection level, and scattering from above this height may be neglected. In the horizontal plane, in order not to waste computer time calculating scattering from the fringes of the Gaussian, the LIE is cut off at the ellipse defined by $\delta N_e = \delta N_e^0/e$. The maximum electron density perturbation δN_e^0 at the LIE centre is taken to be 1.5 el/cc, in good agreement with precipitating electron fluxes actually observed on low altitude orbiting satellites.

3. Scattering theory and implementation

The linear Born theory of 3D VLF scattering from an ionospheric plasma perturbation is fully described in Nunn (1997). The Born approximation involves assuming that the total incident field at a given point in the LIE is the zero order field As shown in Nunn (1997) a better linearisation may be achieved by assuming that $\mathbf{D}' = 0$ within the LIE rather than $\mathbf{E}' = 0$. This takes into account the polarisation field generated within the LIE, and results in the following expression for $\mathbf{J}_{\text{eff}}(\mathbf{r})$.

$$\mathbf{J}_{\text{eff}}(\mathbf{r}) = \frac{jk^2 X'}{\omega\mu_0}\left[1 + (1-\alpha)X_0 + \alpha X\right]^{-1}(1 + X_0)\mathbf{E}_0 = \sigma \boldsymbol{E}_0 \quad (4)$$

The quantity α is a factor dependent on the geometry of the LIE. In the current simulations, the LIE resembles a flat dielectric disc. By analogy with the isotropic problems of a dielectric slab or sphere in an applied electric field a suitable choice for α is 0.66, although the results of this simulation are scarcely affected by the choice of parameter α.

The current version of the code neglects all components of σ except the zz component. When the transmitter and receiver are both ved's (vertical electric dipoles), this is amply justified to an overall accuracy of an order of a few percent. A more advanced version of this code due to R. Yeo (Clilverd et al., 1999) uses the full σ matrix and by means of the USN NOSC LWPC code (long wave propagation code) also permits an inhomogeneous background ionosphere. Clearly for large LIE patches and/or patches with large δN_e the Born approximation will break down, since the total field at a point in the LIE will not be well approximated by the zero order incident field. Using a 2D Finite Element modelling of VLF scattering it was shown in Nunn et al. (1998) and Baba et al (1998) that for an LIE with horizontal dimensions ~100 km the Born approximation fails for maximum electron density perturbations >6 el/cc. The dominant cause of non-Born behaviour is the progressive exclusion of the incident field from the interior of the LIE due to the classic and well known skin depth effect. When the skin depth is of the order of the vertical dimension of the LIE, then non-linear scattering may be anticipated. The current version of the code calculates an attenuation factor for the incident field inside the LIE due to the skin depth effect, but in the present calculations δN_e is small and the situation is close to linear Born scattering.

The physical volume of the LIE is enclosed by a 3D spatial box, containing a grid of ~100 × 300 × 60 points in x, y, z, respectively. The incident field $\mathbf{E}_0$ is computed at each elemental point, from which the source current $\mathbf{J}_{\text{eff}}$ may be derived. The scattered field is that radiated by the source current field $\mathbf{J}_{\text{eff}}(\mathbf{r})$ located within the body of the LIE. It is clearly required to calculate the transmissivity between the transmitter and every point in the LIE, as well as between every point in the LIE and the receiver. The transmissivity of the direct path from transmitter to receiver is also required. To handle the subionospheric VLF propagation problem the code uses the well-known modal theory of Wait (1970). At short ranges

<50 km the modal expansion does not provide a satisfactory description of the field **E(r)**, and so this code will not be valid if the LIE is closer to either the transmitter or receiver than 50 km. The code uses the NOSC MODEFNDR (Modefinder, Morfitt and Shellman, 1976) suite of programs in order to compute VLF modal propagation. These codes incorporate Earth curvature and an anisotropic ionosphere, and a ground plane of specified conductivity and dielectric constant. These programs have the disadvantage of being somewhat inaccurate at very high altitudes >85 km, and future research involving either short ranges or scattering from high altitudes will require that transmissivities be calculated from a full wave VLF program. For the NWC transmitter, MODEFNDR returns 18 modes, both TM and TE. All these are used in the propagation calculations. Even for the scattered field, the amplitudes of the highest order modes are negligible, thus confirming the validity of the modal expansion.

4. Results of modeling horizontally extensive LIEs

For NWC transmissions, we now compute the amplitude and phase Trimpis that will be seen at Dunedin, assuming that the receiver is at zero altitude and represents a vertical electric dipole antenna measuring *Ez*. In accordance with the above discussion the LIE is elliptically shaped, with length 600 km and width 200 km, and orientated E/W, and assumed to be inclined at 25° to the GC path connecting NWC to Dunedin. In order to agree with the observed precipitated particle fluxes the peak electron density enhancement is taken to be 1.5 el/cc. The LIE centre is successively placed on a grid of points covering the corridor between transmitter and receiver, and the Trimpis computed in each case.

This version of the code invokes a first order correction to the Born approximation, and multiplies the incident field by a complex attenuation factor, which is the 'skin depth' attenuation $\Xi(\mathbf{r})$ integrated from the

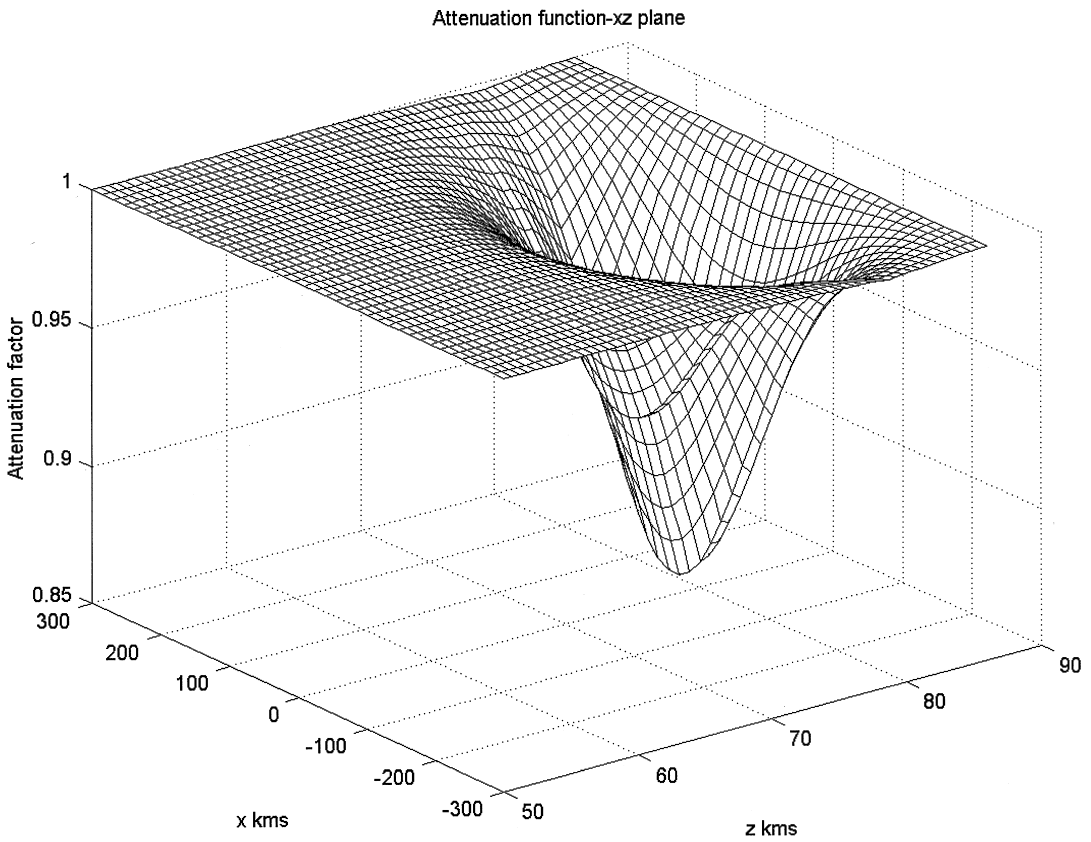

Fig. 1. Surface visualisation of incident field attenuation function (skin depth effect) in the horizontal x', z' plane at $z = 75$ km.

nearest outer boundary of the LIE. Fig. 1 plots $|\Xi(\mathbf{r})|$ in the $x'z$ plane for $y' = 0$. Even in the centre of the LIE, the attenuation is only about 0.89, and so for weak LIEs the Born approximation is nearly valid.

Fig. 2 shows a contour plot of a negative amplitude Trimpi plotted in the x, y plane. Here the vertical axis connects NWC with Dunedin, with the origin at NWC. The horizontal axis is orthogonal with $y = 0$ on the GC path. The range of values on the vertical axis starts at 200 km from NWC and stops at 200 km from Dunedin. Significant amplitude Trimpis are seen in a corridor centred on the GC path. This corridor has a surprisingly constant width of 170 km either side of the GC path. The amplitude Trimpis are consistently negative as observed for long paths, and attain a maximum value ~ -0.5 dB, which is a very typical figure in good accord with observations. Clearly large weak LIEs with electron density enhancements ~ 1.5/cc are able to produce Trimpis of the size observed. Significant peaks occur mid path, with further peaks at distances of ~ 750 and 1250 km from either end. This functional form is due in part to destructive interference between fields scattered from different parts of the LIE, and also partly due to modal interference in both the *scattered* field and the zero order field incident on the LIE. Destructive modal interference is particularly marked when the two scatter path lengths are 2000 and 3800 km. It might be expected that Trimpis would become very large when the LIE is near either end. However, destructive interference in fields scattered from different parts of the large LIE ensures that this is not the case. Regions of positive amplitude Trimpis will be seen near the transmitter (TX) or receiver (RX). The large Trimpis observed mid path are due to (a) minimal destructive interference due to scattering from different parts of the LIE and (b) favourable modal phasing when the TX → LIE and LIE → RX paths have the same length. It might be anticipated that in the presence of an inhomogeneous background ionosphere this central peak may disappear.

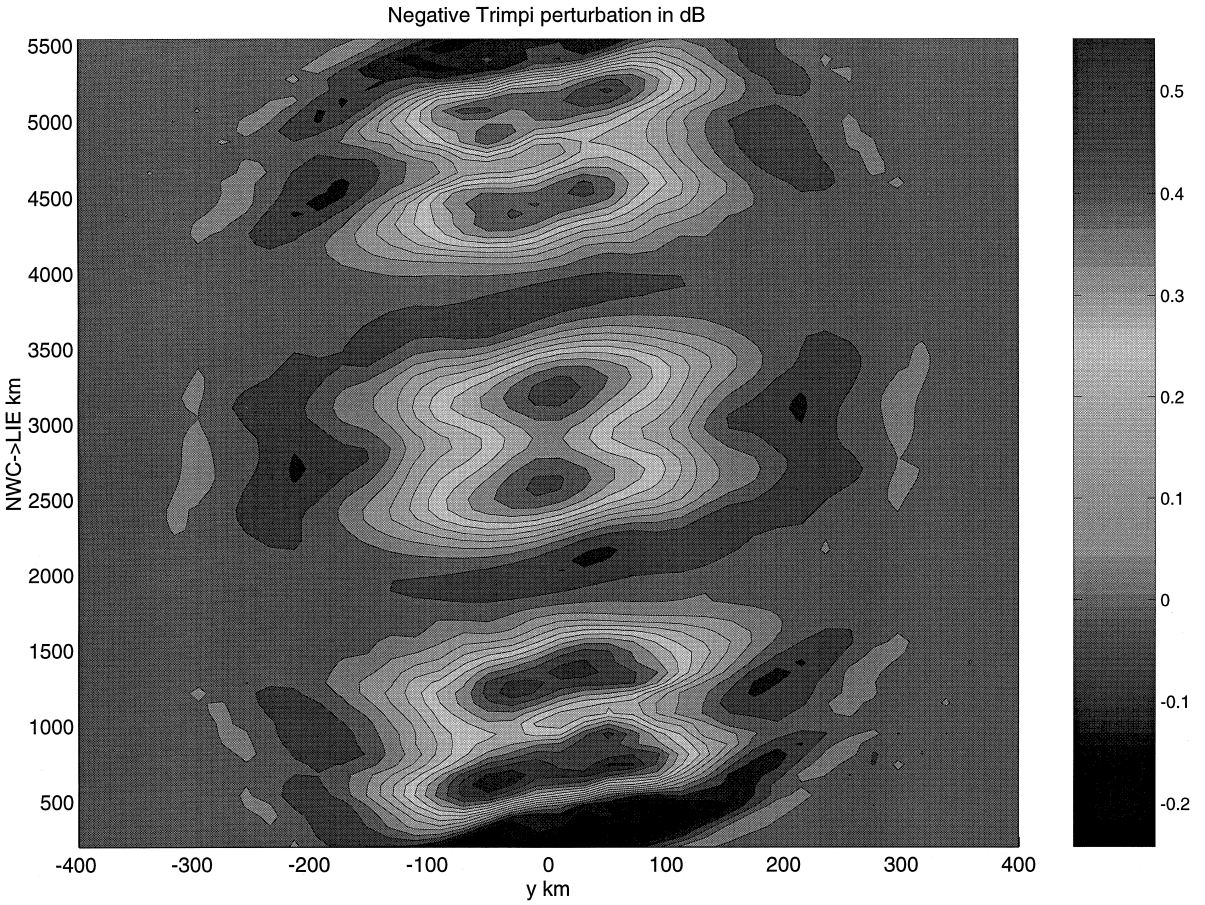

Fig. 2. Contour plot of negative amplitude trimpis at Dunedin as a function of LIE centre coordinates x, y. The consistently negative Trimpis ~ -0.3 dB are in good accord with observations.

The reader will notice the close symmetry present in the graph. The Trimpi at (x, y) is nearly the same as that at $(5740-x, -y)$ (in km). This is to be expected from geometrical considerations. Clearly the angle subtended by the ellipse major axis to the GC path ($\sim 25^\circ$) is a critical parameter. Some numerical experiments have been performed in which the LIE is progressively rotated. The results obtained were fairly predictable. With the LIE major axis parallel to the GC path a larger Trimpi results, but the width of the corridor for LIE centre location in which significant Trimpis are observed becomes narrower. Conversely, for an LIE inclined at right angles to the GC path Trimpi values are smaller, but the corridor is wider.

Fig. 3 plots calculated phase Trimpis in degrees as a function of LIE centre coordinates x and y. This is presented as a surface visualisation. The phase Trimpis are consistently positive with maximum values $\sim 4^\circ$, in good agreement with observations. The functional dependence of phase Trimpi on x, y is dictated mainly by scattered amplitude, and is thus similar to that in Fig. 3. Fig. 4 plots the magnitude of scattered field in dB relative to the zero order field at Dunedin. The scattered signal strength peaks at -30 dB, and has peak values mid path and at 300–1500 km distance from either the RX or TX. The LIE corridor giving significant scattered amplitude is about 150 km either side of the GC path. Observations have been reported of very large Trimpis with scattered strengths ~ -15dB. These presumably arise for large LIEs that are very close to or overlap the receiver or transmitter site. We cannot model these cases without resort to a full wave propagation code.

Fig. 5 is a MATLAB surface visualisation of scatter phase as a function of LIE position coordinates x and y. The plot is limited to ± 150 km in the y coordinate. Beyond this corridor the plot becomes disorderly, since scatter phase winds round quickly as expected for the increasing scattered signal path lengths. Scatter phase has peak positive values $\sim 155^\circ$, but is remarkably flat in the x,y plane maintaining a range of values 130–150°, but in the regions where scattered strength exhi-

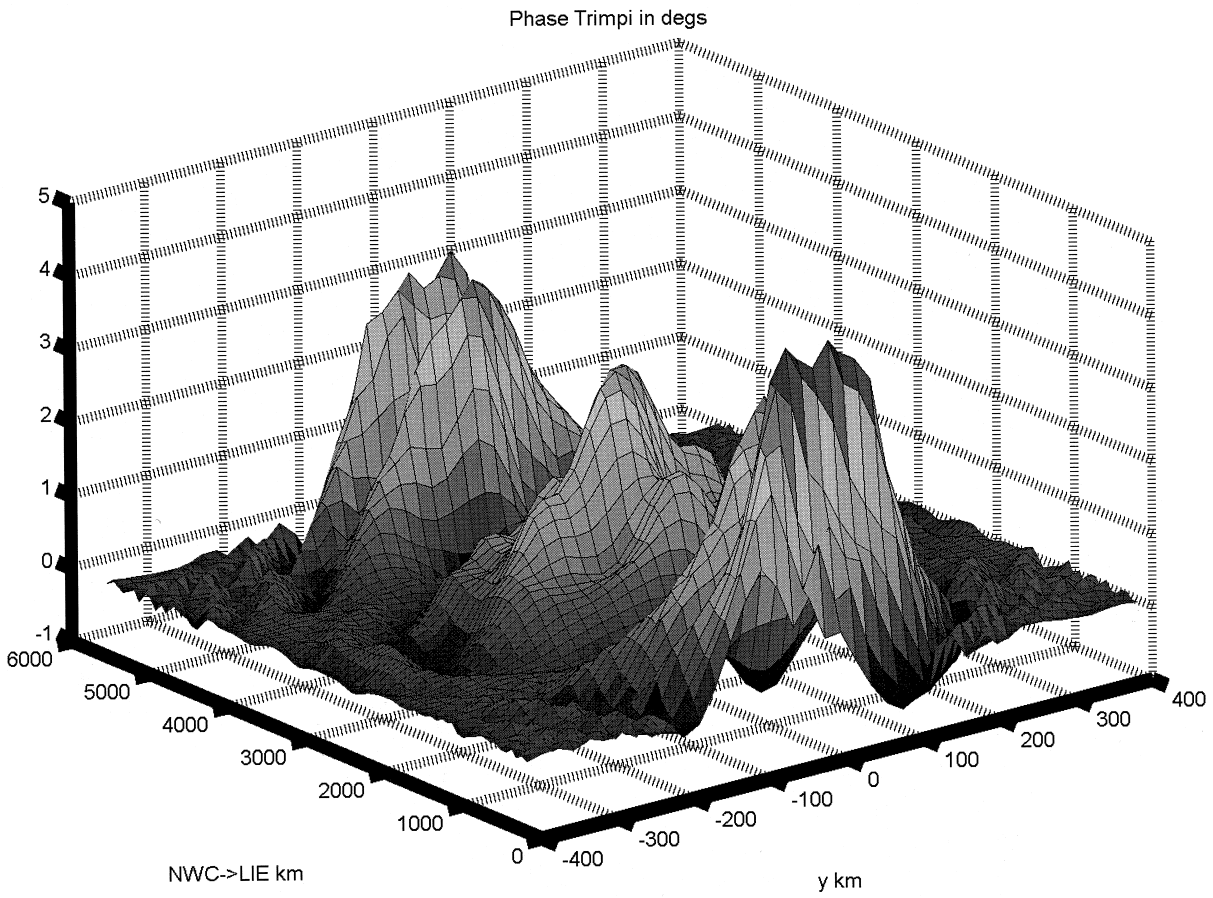

Fig. 3. Phase Trimpis at Dunedin as a function of LIE centre coordinates. This is shown as a MATLAB surface visualisation. The generally positive values $\sim 4^\circ$ are in good accord with observations.

bits a pseudo null the phase winds round a cycle. The dominant scattering comes from portions of the LIE that still overlap the GC path — hence the consistency of scatter phase. When $|y|$ reaches a value where no part of the LIE intersects the GC path, then the scattered amplitude falls rapidly and the scatter phase winds round. Thus on the whole, for LIE centre locations where scattered signal strength is observable, scatter phase is consistently in the same quadrant with values 130–150°. We thus expect invariably to see negative amplitude and positive phase (−+) Trimpis, regardless of LIE location. This is in very good agreement with observations on long homogeneous over-sea paths, such as that from NPM Hawaii to Palmer, Antarctica. Scatter phase consistency is very much a characteristic of large LIEs. It is obvious that smaller LIEs are able to exhibit a full range of scatter phase since off GC path Trimpis will be observable. The main argument against small intense LIEs is that the observed particle fluxes are not consistent with the required electron density perturbations. Of course there now remains the problem of explaining sets of observations where scatter phase is *not* in the (−+) quadrant. This may be due to modal coupling on the direct path due to ionospheric inhomogeneity, multiple/structured LIEs, scattering from close or co-incident LIEs or from smaller structures such as sprites. Some comment needs to be made concerning the actual value of scatter phase predicted. It was shown by Nunn (1997) that a small low altitude resistive scatterer on the GC path should give a scatter phase ~225°, provided that modal interference effects are not prominent. However, due to the extra scattered field path length implied by scattering at altitude, as well as the extra average path length due to the large physical size of the LIE, we find a scattered phase about a 1/4 of a cycle less, and in the region of 135°. Paradoxically this is the scatter phase predicted by the expression of Wait (1970) used by Poulsen et al. (1990, 1993), which assumes that the scale length of the LIE is $\gg \lambda$.

The current field $\mathbf{J}_{\text{eff}}(\mathbf{r})$ within the LIE region radiates scattered field energy into all modes allowed in the

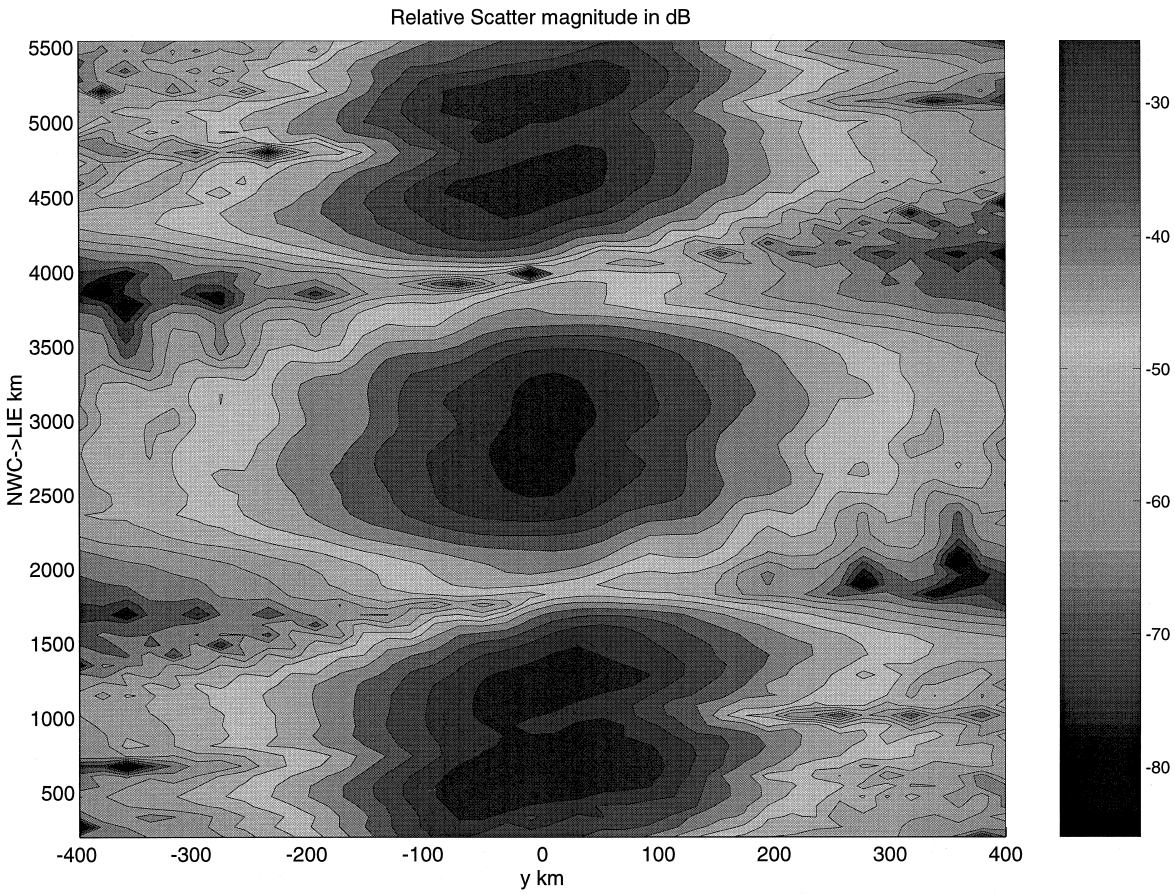

Fig. 4. Contour plot of the magnitude of scattered field at Dunedin, as a function of LIE centre coordinates x, y. The units are in dB relative to the direct signal at Dunedin.

Earth-ionosphere waveguide. In Nunn (1997) a modal scattering matrix for a single point scatterer was defined as follows. The scatterer was assumed to be an elementary volume in the LIE with the appropriate value of conductivity tensor.

$$\eta^{mm'}(\mathbf{r}) = \tilde{c} \cdot \lambda_{33}^{m'} \sigma_{33}(\mathbf{r}) \Gamma_z^m(z) \Gamma_z^{m'}(z) \tag{5}$$

where

$$\tilde{c} = \frac{\mu_0 \omega}{h\sqrt{2\pi k}} \mathrm{e}^{\,j5\pi/4} \tag{6}$$

If mode m only is incident on a point scatterer at $\mathbf{r} = (x, y, z)$, then $\eta^{mm'}$ indicates the modal amplitude of mode m' in the scattered field. In the above expression, h is the ionospheric reference height = 50 km, $\lambda_{33}^{m'}$ is the excitation for the Ez field for a vertical dipole, and $\Gamma^m(z)$ is the height gain function for mode m for the field Ez. The quantity σ_{33} is the zz component of the conductivity tensor.

Fig. 6 plots the magnitudes of the diagonal elements of the modal scattering matrix η^{mm} (labelled as matrix M on the plot) for the three dominant TM modes, which in MODEFNDR order are mode 3, mode 1 which is the Earth detached mode with low excitation factor, and mode 5 which is the next TM mode. Note that the quasi TE mode 2 is not insignificant in this instance, and is of course included in all the computations. The η^{mm} are plotted as a function of z in arbitrary magnitude units. The strongest scattering comes from a height ~72 km. The largest element is η^{55} followed by η^{33}. Diagonal scattering of the Earth detached mode 1 η^{11} is low, partly because of its low excitation factor. Fig. 7 plots the dominant six off diagonal components of the modal scattering matrix η (labelled as M) as a function of z, using the same normalisation. These also peak at about 72 km altitude, and are of the same order of magnitude as the diagonal components, which is hardly surprising for a point scatterer.

It is of some interest to plot the phase of η^{mm} (labelled as M) for the dominant three diagonal

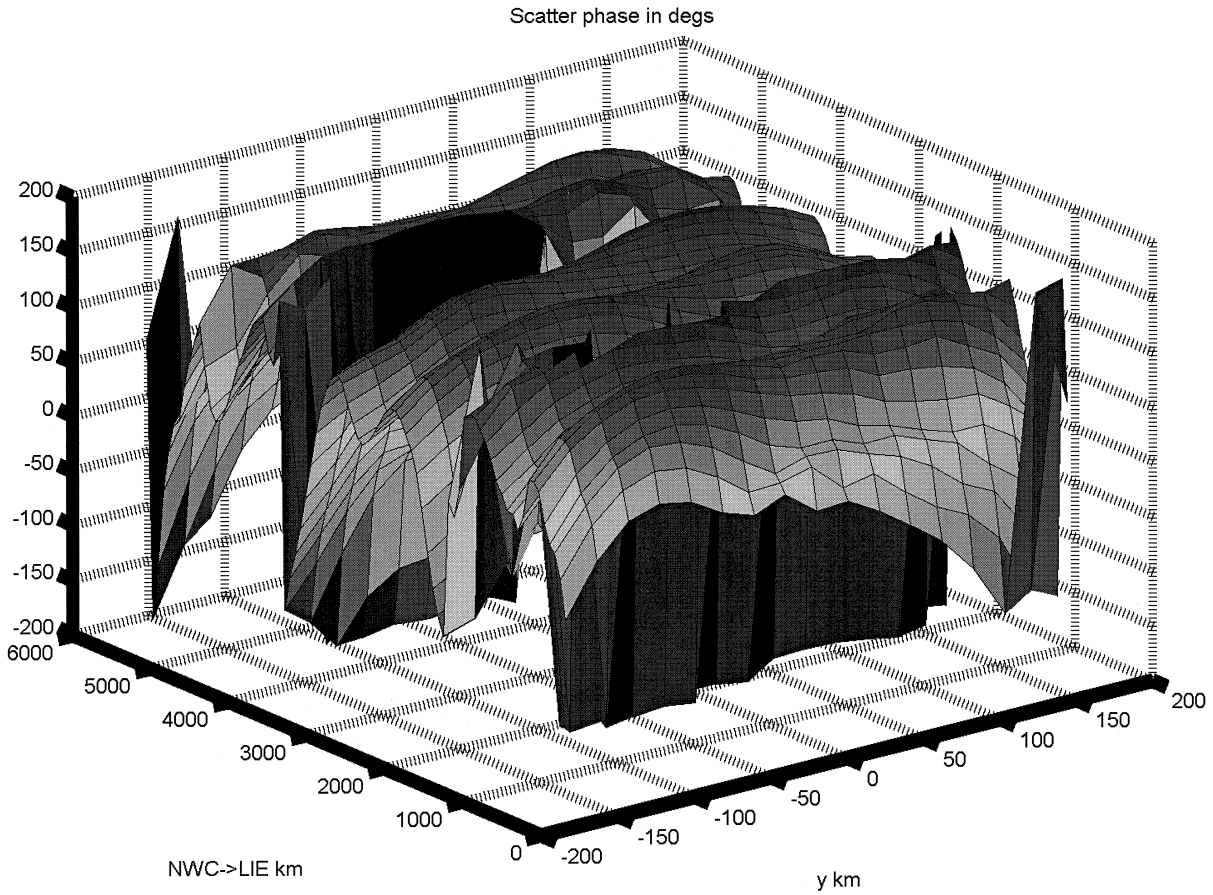

Fig. 5. Scatter phase in degrees at Dunedin as a function of LIE centre coordinates. This is shown as a MATLAB surface visualisation. The remarkable constancy in the range 120–155° (the (− +) quadrant) will be noted.

components, as a function of height z. This is shown in Fig. 8, where the solid line is $\arg(\eta^{33})$, the dashed line is $\arg(\eta^{11})$, and the remaining dot-dash line is $\arg(\eta^{55})$. These arguments would be the Trimpi scatter phases of a point scatterer on the GC path, if all other modes were ignored. The fundamental scatter phase equals arg(c) which is 225°. However, the scatter phase will not be exactly equal to this figure even at low altitude because the height gain functions, the zz component of conductivity tensor and the excitation factors are all complex, though close to real. Inspection of the graph shows that the arguments are all in the region of 225° at low altitudes, though $\arg(\eta^{55})$ winds through a cycle at 52 km in the region of a 'null' in the height gain function. All the phase arguments are seen to decrease with height which is completely intuitive as one expects extra phase lag as the scatterer increases in height and enters the ionospheric plasma.

We next derive the modal scattering matrix for a column of enhanced ionisation, which is obtained by integrating Eq. (5) over z

$$\bar{\eta}^{mm'}(x, y) = \int \eta^{mm'}(\mathbf{r})\, \mathrm{d}z \tag{7}$$

$$\bar{\eta}^{mm'}(x, y) = \tilde{c} \cdot \lambda_{33}^{m'} \cdot \int \sigma_{33}(x, y, z) \Gamma_z^m(z) \Gamma_z^{m'}(z')\, \mathrm{d}z \tag{8}$$

Thus, for a *column* the modal scattering matrix is proportional to the integral over height of the product of the Ez height gain functions of the incoming and outgoing modes m and m', times the zz component of effective conductivity tensor.

It was pointed out by Wait (1980, 1995) that intermodal scattering would be significant if the conductivity $\sigma_{33}(z)$ is noticeably a function of z or limited to a finite range of z. This is certainly the case here since $\sigma_{33}(z)$ is sharply peaked about $z = 73$ km. Fig. 9 plots

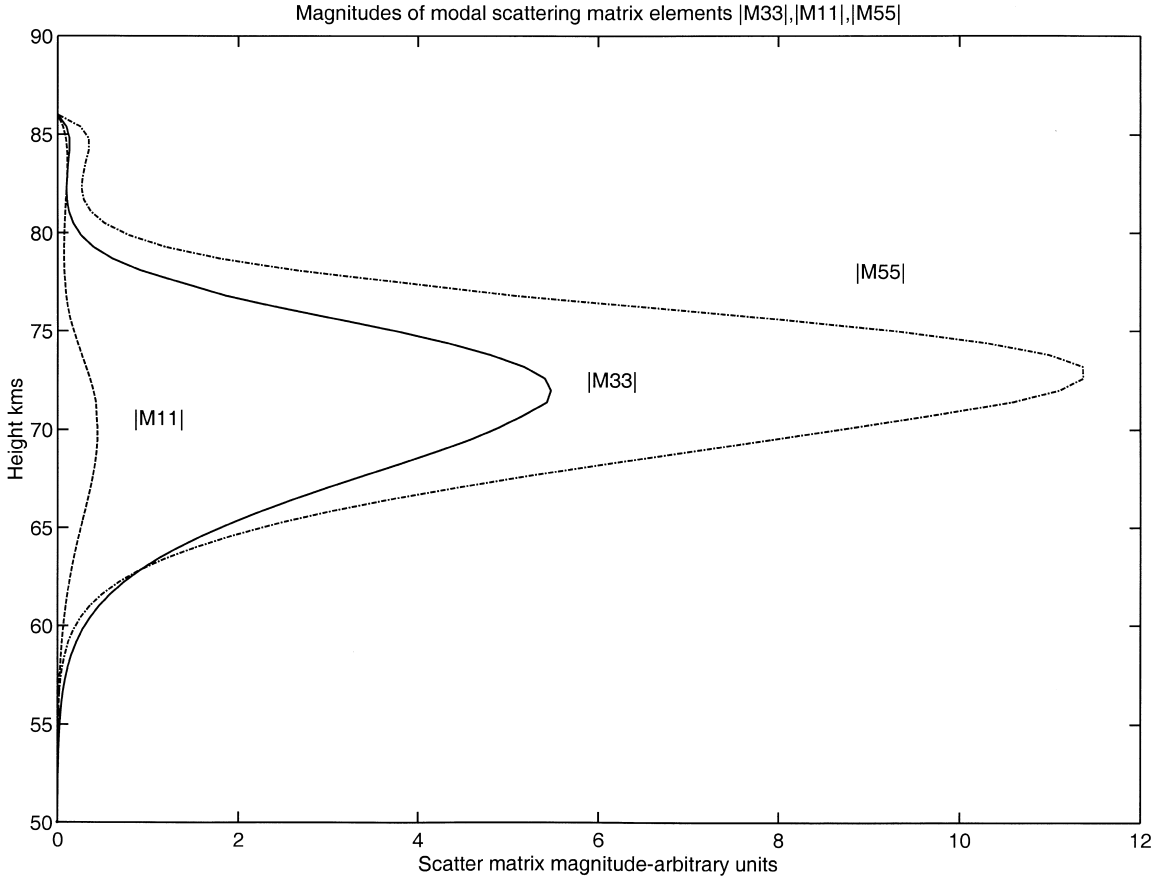

Fig. 6. Magnitudes of diagonal elements of the modal scattering matrix for the three dominant TM modes. This is for a point scatterer and is given in arbitrary units as a function of height. Most scattering comes from altitudes around 72 km.

the magnitudes of the column modal scattering matrix for the six dominant TM modes (labelled as matrix M on the graph). The values are normalised to $|M_{33}|$. The representation is as a MATLAB surface view. The MODEFNDR modes 1, 3, 5, 7, 9, 11 are renumbered 1–6. The right-hand axis represents mode m and the left-hand m'. The scattering is from mode m to m'. The significance of intermodal scattering is apparent at once, particularly the scattering from the Earth detached mode 1 to TM modes 3, 5, 7, 9. Clearly if $\sigma_{33}(z)$ is independent of height z, then the off diagonal elements of the modal scattering matrix will be small due to the near orthogonality of the height gain functions. In the case of sprite columns the scatterer is more extended in z; it has been noted that the modal scatter matrix is more diagonally dominant in this case (Rodger and Nunn, 1999; Nunn and Rodger, 1999).

A final question that might be asked is: what is the modal scattering matrix for the LIE as a whole? We have calculated this as follows. It is assumed that only mode m, with unit amplitude on the ground ($z = 0$), is incident on the LIE from the direction of NWC. We then compute $R_{mm'}$, the complex amplitude of mode m' in the scattered field at $z = 0$ at a suitable range of 1200 km, which is the LIE-receiver range giving maximum Trimpis for the path NWC to Dunedin. Since the modal scattering matrix must now, of necessity, be computed at a medium range, the structure looks a little different from that of the point and column scatter matrices. The higher order modes are of course now subjected to considerable attenuation in propagating out to the observation point.

For the E/W LIE 600 km long and 200 km wide, Fig. 10 shows a MATLAB surface view of $|R_{mm'}|$ in the mm' plane, where the scattering is from mode m to mode m'. The modes labeled 1–5 are the dominant MODEFNDR TM modes 1, 3, 5, 7, 9 in that order, where mode 1 is the semi-Earth detached mode. To facilitate detailed inspection we present the coefficient magnitudes in Table 1. The matrix has a banded structure, with large diagonal elements and not insignificant elements adjacent to the diagonal for which $m' =$

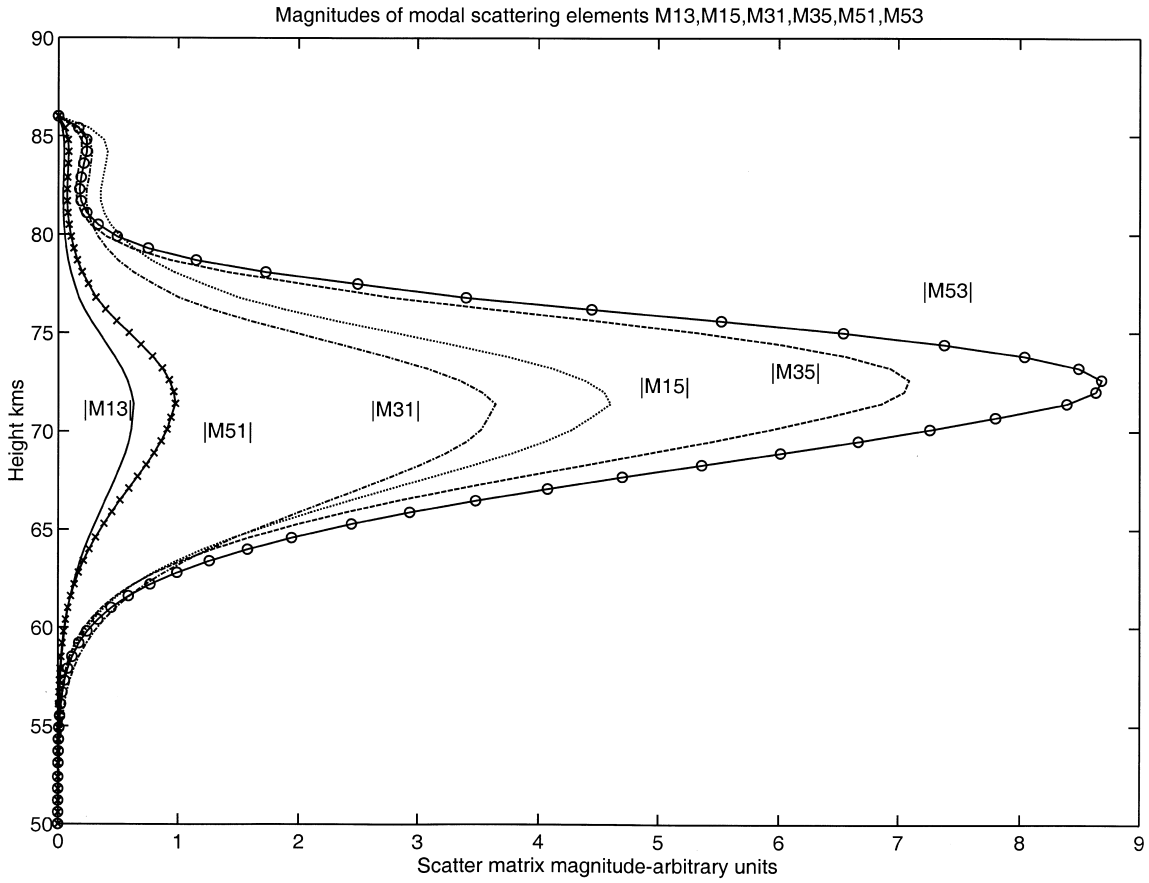

Fig. 7. Magnitudes of off-diagonal elements of the modal scattering matrix as a function of height. These are shown for the six elements corresponding to the three dominant TM modes. The magnitudes are comparable with those of the diagonal elements.

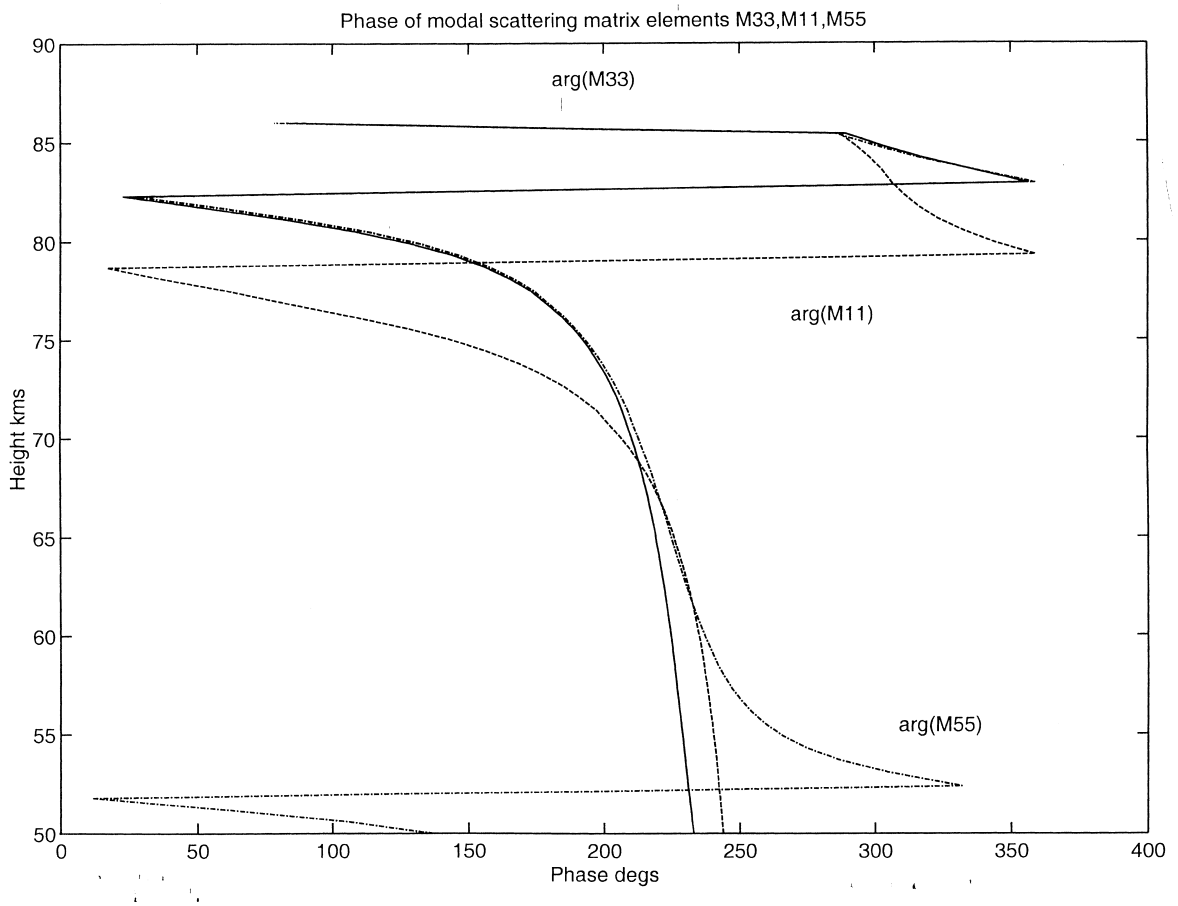

Fig. 8. Arguments of the diagonal elements of the modal scatter matrix for a point scatterer, shown as a function of height for the three dominant TM modes. Note the expected values of approximately $+225^{\circ}$ at low altitudes and the steady decrease with altitude.

$m \pm 1$. In particular, the cross coupling between dominant TM modes 1 and 3 is very significant. Since these modes have a differential in parallel wave number of only 0.8%, it is apparent that extremely large LIE sizes are required to eliminate this cross coupling. The further one goes from the diagonal the smaller the elements become, which is entirely as expected since the extent of dephasing of intermodal scattering across the LIE will be greater the larger the difference in parallel

Table 1
Magnitude modal scattering matrix $|R_{mm'}|$ ($\times 1000$) for the entire 600×200 km elliptical LIE. Scattering is from mode m to m'. Range 1200 km

	To mode M'				
	1	3	5	7	9
From mode M					
1	9.37	20.3	10.0	0.40	0.0095
3	6.28	15.3	9.7	1.02	0.028
5	5.7	17.5	18.7	6.07	0.225
7	0.95	4.6	11.1	13.3	2.13
9	0.086	0.64	0.83	4.2	7.64

Table 2
Scatter matrix $|R_{mm'}|$ ($\times 1000$) for a very large LIE, dimensions 1200×400 km. Range 1200 km

	To mode M'				
	1	3	5	7	9
From mode M					
1	19.2	35.7	1.35	1.13	0.13
3	11.1	31.4	8.1	0.37	0.21
5	0.98	15.6	38.3	1.2	0.4
7	1.47	1.49	1.72	27.3	1.06
9	0.16	1.60	1.30	1.90	15.5

wave number is. Clearly for an LIE that is 600 × 200 km intermodal scattering is important and may not be neglected.

We now repeat these calculations for an LIE twice as large, i.e. 1200 × 400 km. Table 2 presents the numeric data for $|R_{mm'}|$. Intermodal scattering is somewhat further reduced, and the matrix is more diagonally dominant. However, coupling between the two dominant TM modes 1 and 3 is still very significant.

Much of the Trimpi data available has been observed on the Antarctic peninsula at Faraday and Palmer stations, looking at long range homogeneous over sea paths such as from NPM Hawaii. Trimpi simulations for large weak LIEs have been made for the path NPM to Faraday. The calculated Trimpis, presented as a function of LIE-RX range, are fairly similar to those on the path NWC-Dunedin. In this case the incident signal on the LIE is more unimodal and there is less intermodal interference in the scattered signal. For the same LIE geometry the scattered signal power is very similar in magnitude and functional dependence on RX-LIE range. However, the scatter phase for NPM-Faraday is more positive (advanced) than for NWC-Dunedin, by some 10° on average, and shows smaller oscillations due to multimodal effects. Recent observations at Faraday report the occurrence of very large Trimpis, $\sim -1 \rightarrow -2$ dB in amplitude and ~10–20° in phase (Lev-Tov et al., 1996). Such observations have been successfully modelled using this 3D Born code, assuming very large LIE patches ~1200 km long orientated along the GC path.

5. Conclusions

In this paper we have used a 3D Born 'weak scattering' code to compute VLF classic Trimpis produced by large elliptically shaped LIEs of dimensions 200 × 600 km. The peak electron density perturbation has been chosen to be small, ~1.5 el/cc. This figure is consistent

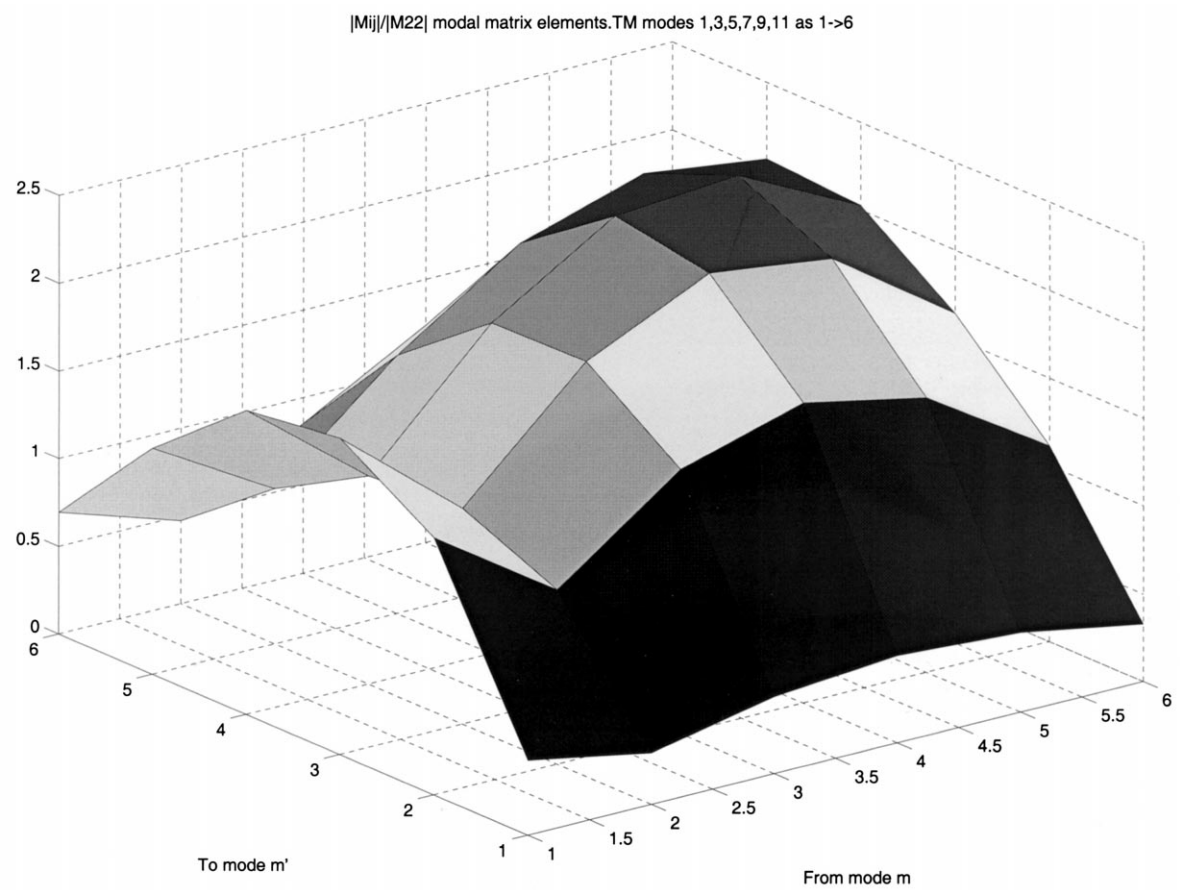

Fig. 9. For a column scatterer, magnitudes of the modal scatter matrix for the first six TM modes. The visualisation is as a MATLAB surface. Significant intermodal scattering is obvious, particularly from Earth detached mode 1.

with observed fluxes of precipitating energetic electrons at the top of the ionosphere. The computed Trimpis are of order −0.4 dB and +4° of phase, figures in good accord with experimental observations. More remarkably, regardless of LIE location, it was found for these large weak LIEs that the scatter phase was remarkably consistent in the range 120–155°, predicting a strong preponderance of negative amplitude positive phase Trimpis. This is also in excellent accord with observations of Trimpis on long oversea (homogeneous) paths.

The apparent discrepancy between observed duct sizes and the much larger postulated sizes of precipitation patches may be readily explained. Numerical and theoretical studies of non-linear wave–particle interactions in the equatorial zone — particularly simulations of triggered VLF emissions and chorus — have shown that there is a great excess of power input in the one dimensional (ducted) formulation. It is very clear that the non-linear resonant particle current field in an interaction region sited in a duct in the equatorial zone will radiate into non-ducted modes, giving rise to a powerful non-linear unducting loss of wave-energy. It is this wave field energy, spilling out of the duct in the equatorial zone, that will cause precipitation over a much wider region than the true duct, as defined by the enhanced plasma density. It is indeed interesting that theoretical and numerical studies from the field of Trimpis and plasma simulation should point towards the same conclusion.

Regarding the theory and technique of Trimpi modelling there is room for further improvement in the future. The code of R. Yeo (see Clilverd et al., 1999) already embodies an inhomogeneous background ionosphere using LWPC software, and uses the full conductivity matrix instead of only the *zz* component. The

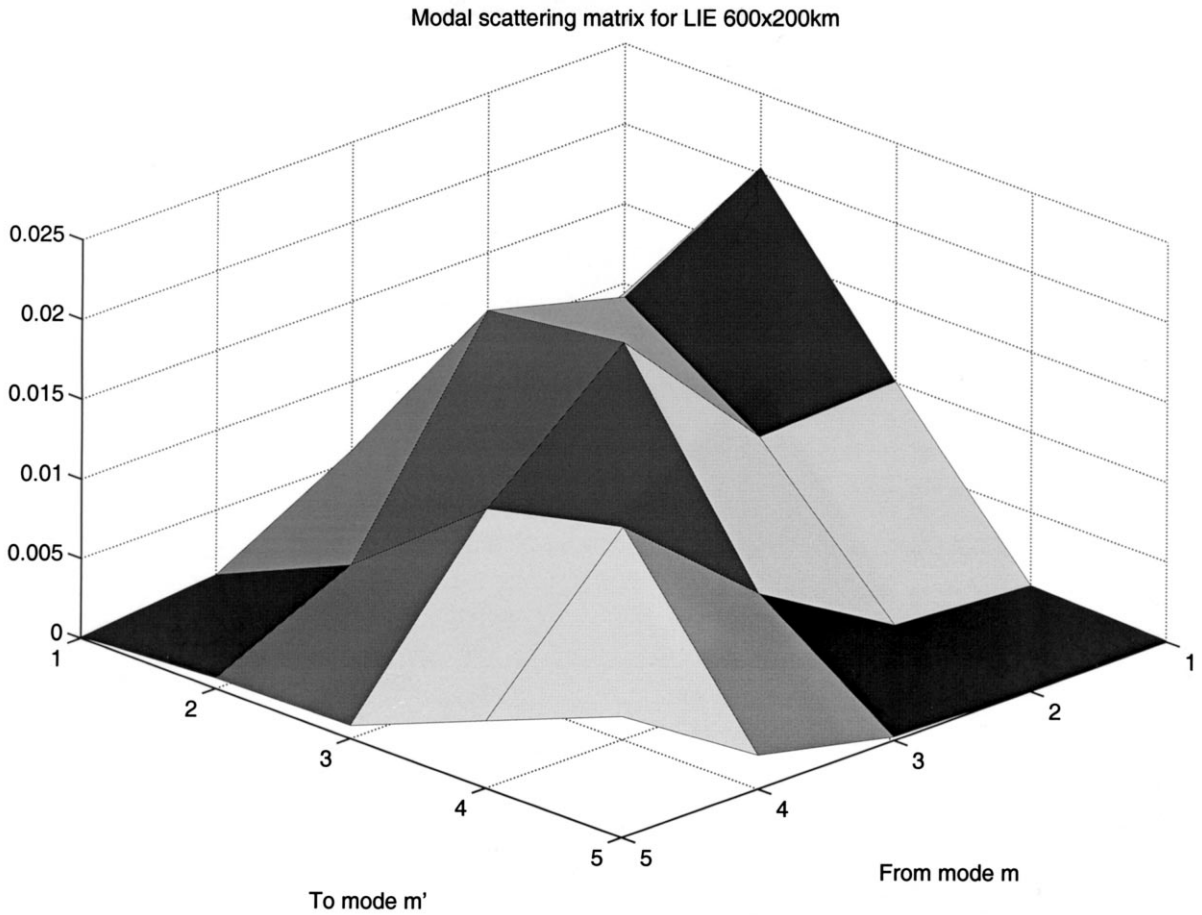

Fig. 10. Plot of magnitude modal scattering matrix $|R_{mm'}|$ (×1000) for the entire 600 × 200 km LIE, at a range of 1200 km. The modes are the first five dominant TM modes returned by MODEFNDR, nos. 1, 3, 5, 7, 9, labelled as 1 → 5. Mode 1 is the Earth detached mode. The matrix has a banded type structure, with significant cross scattering between the dominant modes TM 1 and 3.

next major advance will be to calculate propagation transmissivities from a full wave propagation package. This will enable high altitude scattering to be computed and also allow short ranges < 50 km to be considered. Indeed a full wave package would enable one to compute transmissivities between different parts of the LIE, and thus open the door towards obtaining a rigorous non-Born solution in a recursive manner. The other completely different approach to Trimpi modelling is through the use of the finite element method as pioneered by Baba and Hayakawa (1995, 1996). They have achieved impressive results for a 2D geometry. Work is underway to extend this code to 3D, but this is a difficult task indeed.

Acknowledgements

The authors wish to thank Professor J.A. Ferguson at NOSC San Diego, for permission to use MODEFNDR software. The authors also wish to thank the Faculty of Engineering, Southampton University, for the use of the SG Origin 2000, on which most of the computations were performed.

References

Angerami, J.J., 1970. Whistler duct properties deduced from VLF observations made with the OGO 3 satellite near the magnetic equator. Journal of Geophysical Research 75, 6115–6135.

Baba, K., Hayakawa, M., 1995. The effect of localised ionospheric perturbations on subionospheric VLF propagation on the basis of the finite element method. Radio Science 30 (5), 1511–1517.

Baba, K., Hayakawa, M., 1996. Computational results of the effect of localised ionospheric perturbations on subionospheric VLF propagation. Journal of Geophysical Research 101 (A5), 10985–10993.

Baba, K., Nunn, D., Hayakawa, M., 1998. The modelling of VLF Trimpis using both finite element and 3D Born modelling. Geophysical Research Letters 25, 4453–4456.

Carpenter, D.L., LaBelle, J.W., 1982. A study of whistlers correlated with bursts of electron precipitation near $L = 2$. Journal of Geophysical Research 87, 4427–4434.

Carpenter, D.L., Inan, U.S., Smith, J., 1984. Use of subionospheric Siple transmitter signals to study burst precipitation outside the plasmapause. Antarctic Journal of the US 19, 220–222.

Clilverd, M.A., Yeo, R.F., Nunn, D., 1999. Latitudinally dependent Trimpi effects: modelling and observations. Journal of Geophysical Research 104, 19881–19888 .

Cotton, P.D., Smith, A.J., 1991. Signature of burst particle precipitation on VLF signals propagating in the Antarctic Earth-ionosphere waveguide. Journal of Geophysical Research 96, 19375–19387.

Crombie, D.D., 1964. The effects of a small local change in phase velocity on the propagation of a VLF radio signal. J. Res. NBS.68D (Radio Science).

Dowden, R.L., Adams, C.D.D., 1988. Phase and amplitude perturbations on subionospheric signals explained in terms of echoes from lightning induced electron precipitation ionization patches. Journal of Geophysical Research 93, 11543–11550.

Dowden, R.L., Adams, C.D.D., 1989a. Modal effects on amplitude perturbations on subionospheric signals (Trimpis) deduced from two frequency measurements. Journal of Geophysical Research 94, 1515–1519.

Dowden, R.L., Adams, C.D.D., 1989b. Phase and amplitude perturbations on the NWC signal at Dunedin from lightning induced electron precipitation. Journal of Geophysical Research 94, 497–503.

Dowden, R.L., Adams, C.D.D., 1993. Size and location of lightning-induced enhancements from measurement of VLF phase and amplitude perturbations on multiple antennas. Journal of Atmospheric and Terrestrial Physics 55, 1335–1359.

Friedel, R.H., Hughes, A.R.W., 1999. Characteristics and frequency of occurrence of Trimpi events recorded during 1982 at Sanae Antarctica. Journal of Atmospheric and Terrestrial Physics 52, 329–339.

Helliwell, R.A., Katsufrakis, J.P., Trimpi, M.L., 1973. Whistler-Induced Amplitude Perturbations in VLF Propagation. Journal of Geophysical Research 78 (22), 4679–4688.

Inan, U.S., Carpenter, D.L., Helliwell, R.A., Katsufrakis, J.P., 1985. Subionospheric VLF/LF phase perturbations produced by lightning whistler induced particle precipitation. Journal of Geophysical Research 90, 7457–7469.

Inan, U.S., Carpenter, D.L., 1987. Lightning induced electron precipitation events observed at $L = 2.4$ as phase and amplitude perturbations of subionospheric VLF signals. Journal of Geophysical Research 92, 3292–3303.

Inan, U.S., Knifsend, F.A., Oh, J., 1990. Subionospheric VLF imaging of lightning induced electron precipitation from the magnetosphere. Journal of Geophysical Research 95, 17217–17231.

Leyser, T.B., Inan, U.S., Carpenter, D.L., Trimpi, M.L., 1984. Diurnal variation of burst precipitation effects on subionospheric VLF/LF signal propagation near $L = 2$. Journal of Geophysical Research 89, 9139–9143.

Lev-Tov, S.J., Inan, U.S., Smith, A.J., Clilverd, M.A., 1996. Characteristics of localised ionospheric disturbances inferred from VLF measurements at two closely spaced receivers. J. Geophys. Res 101, 15737–15747.

Lohrey, B., Kaiser, A.B., 1979. Whistler induced anomalies in VLF propagation. Journal of Geophysical Research 84, 5122–5130.

Morfitt, D.G., Shellman, C.H., 1976. MODESRCH, an improved computer program for obtaining ELF/VLF mode constants. Interim report 77T, NTIS, ADA 032473, Naval Electronics Laboratory Center, USA.

Nunn, D., 1984. The quasistatic theory of triggered VLF emissions. Planetary and Space Science 32 (3), 325–350.

Nunn, D., 1997. On the numerical modelling of the VLF Trimpi effect. Journal of Atmospheric and Terrestrial Physics 59 (5), 537–560.

Nunn, D., Baba, K., Hayakawa, M., 1998. VLF Trimpi mod-

elling on the path NWC-Dunedin using both finite element and 3D Born modelling. Journal of Atmospheric and Terrestrial Physics 60, 1497–1515.

Nunn, D., Rodger, C.J., 1999. Modelling the relaxation of red sprite plasma, Geophysical Research Letters 26(21), 3293–3296.

Ondoh, T., 1976. Field-aligned irregularities in whistler ducts as observed by the ISIS satellite. Space Res XVI, 555–559.

Poulsen, W.L., Bell, T.F., Inan, U.S., 1990. Three dimensional modelling of subionospheric VLF propagation in the presence of localised D-region perturbations associated with lightning. Journal of Geophysical Research 95, 2355–2366.

Poulsen, W.L., Inan, U.S., Bell, T.F., 1993. A multiple mode three dimensional model of VLF propagation in the earth-ionosphere waveguide in the presence of localised D-region disturbance. Journal of Geophysical Research 98, 1705–1717.

Poulsen, W.L., Bell, T.F., Inan, U.S., 1993. The scattering of VLF waves by localised ionospheric disturbances produced by lightning induced electron precipitation. Journal of Geophysical Research 98, 15553–15559.

Rodger, C.J., Nunn, D., 1999. VLF scattering from red sprites: application of numerical modelling. Radio Science 34(4), 933–938.

Smith, A.J., Cotton, P.D., Robertson, J.S., 1993. Transient □ 10 s VLF amplitude and perturbations due to lightning-induced electron precipitation into the ionosphere "the Trimpi effect". In: AGARD Conference Proceedings 529, ELF/VLF/LF Radio Propagation and System Aspects, 1–7 August.

Strangeways, H.J., 1997. Whistler ducts and lightning induced electron density irregularities. In: 13th UK National URSI Colloquium, Leicester University, 11–12 September.

Strangeways, H.J., 1999. Lightning induced enhancements of D-region ionisation and whistler ducts. Journal of Atmospheric and Solar-Terrestrial Physics 61, 1067–1080.

Tolstoy, A., Rosenberg, T., Carpenter, D.L., 1982. The influence of localised precipitation induced D-region ionisation enhancements on the sub ionospheric VLF propagation. Geophysical Research Letters 9, 593–596.

Tolstoy, A., 1983. The influence of localised precipitation induced D-region ionisation enhancements on sub-ionospheric VLF propagation. Tech. Rep. BN-1011, University of Maryland, College Park, MD, USA.

Tolstoy, A., Rosenberg, T.J., 1986. Model predictions of sub-ionospheric VLF signal perturbations resulting from localised electron precipitation induced D-region ionisation enhancement regions. Journal of Geophysical Research 91 (13), 13473–13482.

Voss, H.D., Walt, M., Imhof, W.L., Mobilia, J., Inan, U.S., 1998. Satellite observations of lightning-induced electron precipitation. Journal of Geophysical Research 103, 11725–11744.

Wait, J.R., 1970. Electromagnetic Waves in Stratified Media. Pergamon, New York.

Wait, J.R., 1980. Electromagnetic scattering from an isolated irregularity in a tropospheric duct. Acta Physica Austriaca 52, 193–202.

Wait, J.R., 1995. VLF scattering from a column of ionisation in the Earth-ionosphere waveguide. Journal of Atmospheric and Terrestrial Physics 57, 955–959.